Research in Astronomy and Astrophysics, 23:095022 (10pp), 2023 September https://doi.org/10.1088/1674-4527/ace1d5

Performance Analysis and Optimization of a Modified Stewart Platform for the Qitai Radio Telescope

Guljaina Kazezkhan[1], Qian Xu[1,2,3], Na Wang[1,2,3], Fei Xue[1], and Hui Wang[1]
[1] Xinjiang Astronomical Observatory, Chinese Academy of Sciences, Urumqi 830011, China; jaina@xao.ac.cn
[2] Key Laboratory of Radio Astronomy, Chinese Academy of Sciences, Urumqi 830011, China
[3] Xinjiang Key Laboratory of Radio Astrophysics, Urumqi 830011, China
Received 2023 April 17; revised 2023 June 5; accepted 2023 June 25; published 2023 August 21

Abstract

This paper presents a modified Stewart platform that enables precise adjustment of the sub-reflector for the Qitai Radio Telescope (QTT). QTT demands a parallel platform capable of carrying a heavy load (⩾4000 kg), and moving in elevation from 5° to 88° together with the primary reflector while precisely adjusting the sub-reflector's position in five degrees of freedom. To meet these requirements, a modified Stewart platform with two separated actuators is proposed, and the comprehensive performance is analyzed and optimized for practical application. The performance of the modified platform is compared to that of the traditional Stewart platform, and the results demonstrate that the modified platform has superior load-bearing capacity and stiffness over the entire elevation angle with more uniform actuator load and stiffness distributions. These results indicate that the modified Stewart platform is well-suited for practical application in QTT.

Key words: telescopes – methods: analytical – methods: numerical

1. Introduction

The Qitai Radio Telescope (QTT) is a 110 m aperture fully steerable radio telescope that will be constructed in Qitai County of Xinjiang in China (Wang 2014). The telescope will cover the frequency range of 150 MHz–115 GHz. The primary reflector will adopt an active surface adjustment system (Wang et al. 2020). The surface accuracy for the main and sub-reflectors achieves 0.2 mm (rms) and 0.05 mm (rms), respectively, after long-term adjustment, with pointing accuracy better than 2.″5 above the 6 mm observation wavelength (Xu & Wang 2016). It will make contributions to the field of deep space exploration and fundamental science, such as galaxy evolution and gravitational wave detection. To achieve the above objectives, a dual-reflector antenna must maintain a stringent alignment of the sub-reflector concerning the primary reflector (Keshtkar et al. 2017). However, due to the impact of environmental factors such as gravity and temperature, the structural deformation of a telescope can lead to misalignment between the sub-reflector and the primary reflector. To address this issue, a traditional Stewart platform (as illustrated in Figure 1) has been employed as a sub-reflector actuator. This parallel platform with six degrees of freedom (DOF) comprises a base platform and a mobile platform connected by six prismatic actuators with universal joints at the base and spherical joints at the mobile platform. The Stewart platform is a versatile and reliable platform that offers high precision, stability, and durability (Merlet 2006). Its unique design allows for a wide range of applications, making it an essential tool for many industries. In recent times, the Stewart platform has been widely utilized in telescopes to actively adjust the position of the sub-reflector and align it with the primary reflector. There are some well-known successful applications of the traditional Stewart platform for radio telescopes, such as the Large Millimeter Telescope (LMT) (Gawronski & Souccar 2005), Atacama Large Millimeter/submillimeter Array (ALMA) (Wootten & Thompson 2009), Five-hundred-meter Aperture Spherical Telescope (FAST) (Su & Duan 2000), Tianma Radio Telescope (Li et al. 2014), NanShan Radio Telescope (NSRT) (Xiang et al. 2019) and so on. A small number of radio telescopes adopt modified Stewart platforms, such as the Green Bank Telescope (GBT) applying an orthogonal parallel platform with six DOF as a sub-reflector actuator (Prestage & Maddalena 2006). Also in 2006, when the 100 m Effelsberg telescope was upgraded with an active sub-reflector system, an asymmetric Stewart platform was implemented for the sub-reflector to fulfill rigid body position and orientation (Pietzner & Nothnagel 2010).

As diagrammed in Figure 2, a drawback to the traditional Stewart platform design is that, due to interference constraints between the legs, the orientations of the legs cannot deviate far from the z-axis of the manipulator. Since the static force applied by each leg to the mobile platform must act along the axis of the leg, the force capacity in the z-direction is considerably higher than in the x-y plane, and the torque capacity about the z-axis is limited (Stoughton & Arai 1993). Consequently, as the base platform elevates from 90° to 0°, the

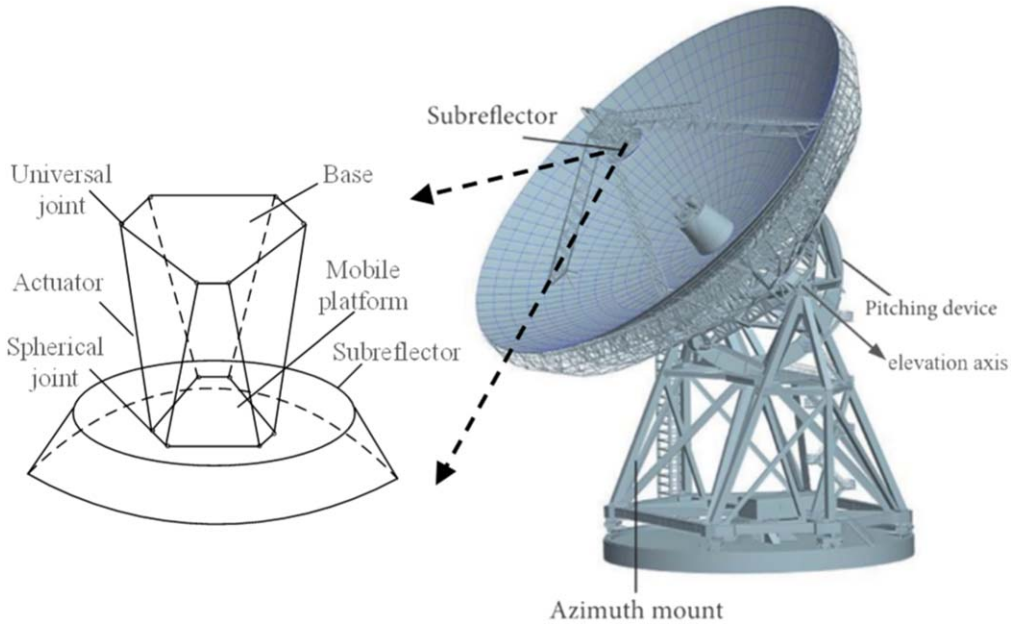

Figure 1. Traditional Stewart platform as the radio telescope sub-reflector actuator.

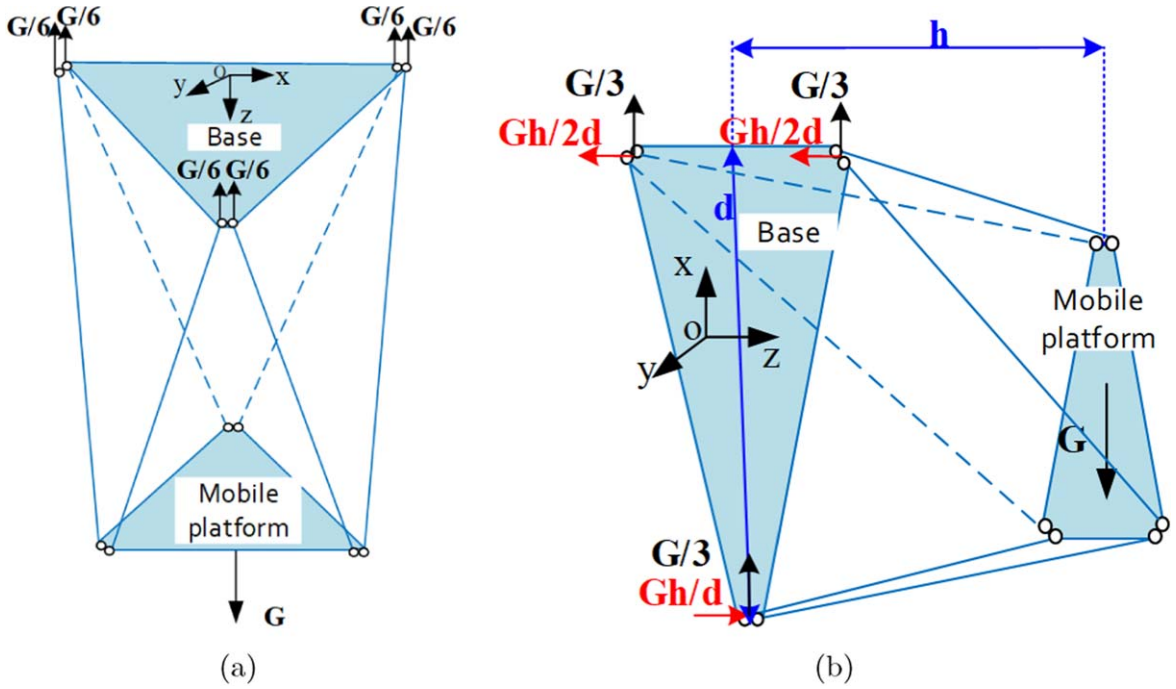

Figure 2. The traditional Stewart platform. (a) Forces on actuator mount point toward the zenith position. (b) Forces on the actuator mount point toward the horizon position.

forces needed to counteract gravity load $\boldsymbol{G}$ at each leg increase. For example, when the antenna is at the zenith position the base is close to the horizontal plane (as in Figure 2(a)), and the force on the actuator mount points is $\boldsymbol{G}/6$; and when the antenna is at the horizon position the base moves close to the perpendicular of the horizontal plane (as in Figure 2(b)), the force on the

actuator mount points is $\boldsymbol{G}/3$ and torque is $\boldsymbol{G}h/2d$, where h is the distance between the base and mobile platform and d is the height of the base platform. It means stiffness of the traditional Stewart platform is best at the zenith position and worst at the horizon position. When using a parallel platform with six DOF on the QTT to adjust the position of the sub-reflector, the platform must follow the primary reflector as it elevates, despite the sub-reflector's significant mass. Therefore, it is essential to optimize the design of the Stewart platform to meet the practical application requirements of a radio telescope.

The primary goal of the optimized design of a parallel platform is to establish reliable and computationally efficient performance indexes that affect the final working performance and optimal design efficiency of the parallel platform. The performance indexes of the parallel platform are mainly focused on kinematics (Hamida et al. 2021; Nunez et al. 2022) and dynamics (Sun & Lian 2018; Jiang et al. 2021), including stiffness, flexibility, accuracy, workspace, and dexterity. Toz and Kucuk designed an asymmetric generalized Stewart platform type parallel manipulator by the type synthesis method (Toz & Kucuk 2013); they optimized the workspace of the Stewart platform under kinematic and geometric constraints, and the optimization results show that the asymmetric generalized Stewart platform has better motion performance than the traditional Stewart platform. Cirillo et al. intended to maximize the payload and minimize the forces used to experiment during positioning (Cirillo et al. 2017). Nayar et al. designed a Stewart platform with six DOF to emulate the behavior of the lander in low-gravity environments (Nayar et al. 2021). There are also many studies on multi-objective optimization methods; Chen et al. proposed a random forest-nondominated sorting genetic algorithm (RF-NSGA-II) multi-objective optimization model with an elite strategy (Chen et al. 2023). Liu et al. applied non-dominated sorting genetic algorithm version II (NSGA-II) for the multi-objective optimization design of the Stewart platform structure, and determined the final solution in a set of Pareto optimized solutions by the global standard method and the minimum power (Liu et al. 2013).

Furthermore, the optimization of the parallel platform for radio telescope applications is challenging due to the requirement of high accuracy, stability, and load-carrying capacity over a wide range of elevation angles. Therefore, the study draws upon previous research on these topics, as well as addressing these challenges by proposing a modified Stewart platform with two separated actuators, an approach that is comprehensively analyzed and optimized for practical application. Finally, to evaluate the performance of the modified Stewart platform, a comparison is made between the performance indices of the modified and traditional Stewart platforms.

Table 1
Design Requirements of QTT Sub-reflector Actuator

No	Item	Range
1	Payload	$\geqslant$ 4000 kg
2	Pitch	$\pm5^\circ$
3	Yaw	$\pm5^\circ$
4	Surge	±300 mm
5	Sway	±300 mm
6	Heave	±300 mm

2. QTT Sub-reflector Adjustment System

QTT is a Gregorian parabolic antenna, the sub-reflector is an aluminum honeycomb sandwich structure with an aperture of 12 m, weight of about 4000 kg and its geometric surface is a hyperboloid of revolution (Xu et al. 2015). The sub-reflector has six DOF, five of which are controlled by the six-DOF parallel platform (the rotation around z-axis is not considered because of the axisymmetrical shape of the sub-reflector). The sub-reflector is supported on the primary reflector by four orthogonal supporting legs and the angles between the elevation axis and legs in the elevation axis plane projection are $\pm45^\circ$, and $\pm135^\circ$, respectively. The elevation range of the primary reflector during observations is 5°–88°. The offset of the sub-reflector causes pointing deviation of the radio telescope, so the sub-reflector must keep a high position and orientation accuracy under multiple working conditions.

QTT adopts a six-DOF parallel platform to obtain desired position and orientation of the sub-reflector by the control of each individual actuator length. The mobile platform of the parallel platform connects the sub-reflector, and the base platform is supported on the primary reflector by four orthogonal supporting legs. Therefore, while adjusting the position of the sub-reflector, the parallel platform allows the primary reflector to elevate 5°–88°. The design requirements of the QTT sub-reflector actuator are shown in Table 1.

3. Description of the Modified Stewart Platform

To design a six-DOF parallel platform for a radio telescope, it is essential to take into account specific requirements, given the numerous actuator arrangement options available. The most critical consideration is that gravity loads will fluctuate as the elevation angle changes within the static configuration. To address this challenge, the modified Stewart platform, displayed in Figure 3, composed of the base platform, the mobile platform, six actuators, and universal (spherical) joints, is proposed. The base platform is fixed and the mobile platform is at the end of the platform. Two platforms are connected by the actuators and the universal (spherical) joints. Symmetrical universal (spherical) joints are positioned around the x_B (x_P) axis and the $x_B(x_P)$ axis is perpendicular to the elevation axis of

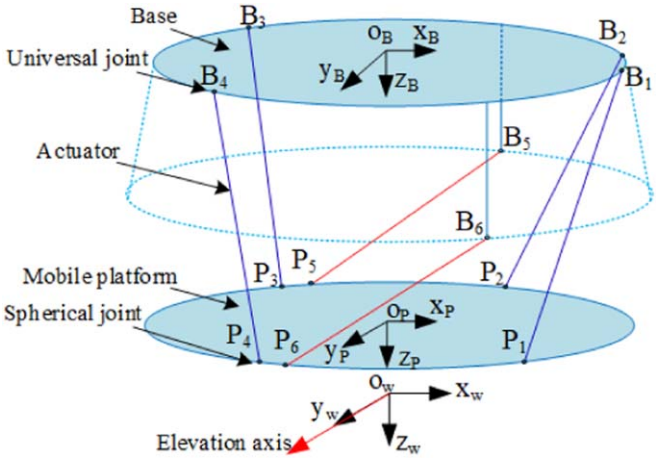

Figure 3. Schematic diagram of the modified Stewart platform.

with its origin, o_P, secured at the center of the platform. The center point of the mobile platform has the coordinates $\boldsymbol{q} = [x, y, z, \alpha, \beta, \gamma]$ where the coordinates $[x, y, z]$ describe the Cartesian position of the mobile platform, and $[\alpha, \beta, \gamma]$ describe the orientation of the mobile platform. The inverse kinematics consists of six nonlinear equations that can be solved uniquely. The equations are

$$l_i \boldsymbol{n}_i^B = \boldsymbol{q}^B + \boldsymbol{R}_P^B \boldsymbol{P}_i^P - \boldsymbol{B}_i^B, \tag{1}$$

where $\boldsymbol{n}_i^B$ and l_i are the unit direction vector and the length of the leg $i\,(i = 1,\ldots,6)$ respectively, $\boldsymbol{q}^B$ denotes the Cartesian coordinates of the center point of the mobile platform relative to the base, $\boldsymbol{P}_i^P$ and $\boldsymbol{B}_i^B$ signify the center points of the universal (spherical) joints in base frame and mobile frame respectively, and $\boldsymbol{R}_P^B$ is the transformation matrix mapping the mobile frame into the global frame. $\boldsymbol{R}_P^B$ is given by

$$\boldsymbol{R}_P^B = \begin{bmatrix} \cos\alpha\cos\beta & \cos\alpha\sin\beta\sin\gamma - \sin\alpha\cos\gamma & \cos\alpha\sin\beta\cos\gamma + \sin\alpha\sin\gamma \\ \sin\alpha\cos\beta & \sin\alpha\sin\beta\sin\gamma + \cos\alpha\cos\gamma & \sin\alpha\sin\beta\sin\gamma - \cos\alpha\cos\gamma \\ -\sin\beta & \cos\beta s \in \gamma & \cos\beta\cos\gamma \end{bmatrix}. \tag{2}$$

the antenna. The six universal joints on the base platform are placed on two planes, and two actuators are positioned closer to being horizontal.

This design achieves a balanced force and torque capacity at various elevation angles and decreases the forces needed to counteract gravity load $\boldsymbol{G}$ at each leg relative to the traditional Stewart platform. Specifically, when the antenna is at the zenith position the base is close to the horizontal plane (as Figure 4(a) illustrates); legs 1–4 bear the load, and the maximum force on actuator mount points is $\boldsymbol{G}/3$; when the antenna is at the horizontal position the base moves close to being perpendicular to the horizontal plane (as Figure 4(b) depicts); legs 5 and 6 bear the load, and the maximum force on actuator mount points is $\boldsymbol{G}/2$. As a result, this configuration effectively distributes the load and minimizes the stress on any one leg, resulting in higher carrying capacity across all elevation angles, and allowing for efficient operation across all elevation angles.

3.1. Inverse Kinematics of the Modified Stewart Platform

In reference to the coordinate system definitions presented in Figure 3, a geodetic reference coordinate frame, $o_w - x_w y_w z_w$, is established at the antenna orientation center with y_w parallel to the elevation axis of the antenna. The base coordinate system, $o_B - x_B y_B z_B$, is attached to the base with its origin, o_B, fixed at the center of the base. The mobile coordinate system, $o_P - x_P y_P z_P$, as the mobile frame, is defined in parallel with the base frame, $o_B - x_B y_B z_B$, but attached to the mobile platform

4. Static Mathematical Model of the Modified Stewart Platform

4.1. Static Load Capacity Evaluation Indices of the Modified Stewart Platform

As demonstrated in Figure 5, $\boldsymbol{F}_P$, $\boldsymbol{M}_P$ represent the resultant force vector and the resultant moment vector applied on the center of the mobile platform, respectively; the reacting forces $\boldsymbol{f}_i$ $(i = 1,\ldots,6)$ act along the axis of the leg. To maintain equilibrium of the mobile platform, the following equations can be obtained as

$$\sum_{i=1}^{6}\left(\boldsymbol{f}_i \cdot \frac{\boldsymbol{P}_i^B - \boldsymbol{B}_i^B}{|\boldsymbol{P}_i^B - \boldsymbol{B}_i^B|}\right) = \boldsymbol{F}_P, \tag{3}$$

$$\sum_{i=1}^{6}\left(\boldsymbol{f}_i \cdot \frac{\boldsymbol{R}_P^B \boldsymbol{P}_i^P \times (\boldsymbol{P}_i^B - \boldsymbol{B}_i^B)}{|\boldsymbol{P}_i^B - \boldsymbol{B}_i^B|}\right) = \boldsymbol{M}_P. \tag{4}$$

Equations (3) and (4) can be rewritten in the form of a matrix equation as

$$\boldsymbol{F} = \boldsymbol{G}_f^F \cdot \boldsymbol{f}, \tag{5}$$

where $\boldsymbol{F} = [\boldsymbol{F}_P\, \boldsymbol{M}_P]$, $\boldsymbol{f} = [f_1\, f_2\, f_3\, f_4\, f_5\, f_6]^T$ and $\boldsymbol{G}_f^F$ can be expressed as

$$\boldsymbol{G}_f^F = \begin{bmatrix} \boldsymbol{n}_1^B & \boldsymbol{n}_2^B & \cdots & \boldsymbol{n}_6^B \\ \boldsymbol{R}_P^B \boldsymbol{P}_1^P \times \boldsymbol{n}_1^B & \boldsymbol{R}_P^B \boldsymbol{P}_2^P \times \boldsymbol{n}_2^B & \cdots & \boldsymbol{R}_P^B \boldsymbol{P}_6^P \times \boldsymbol{n}_6^B \end{bmatrix}_{6\times 6}. \tag{6}$$

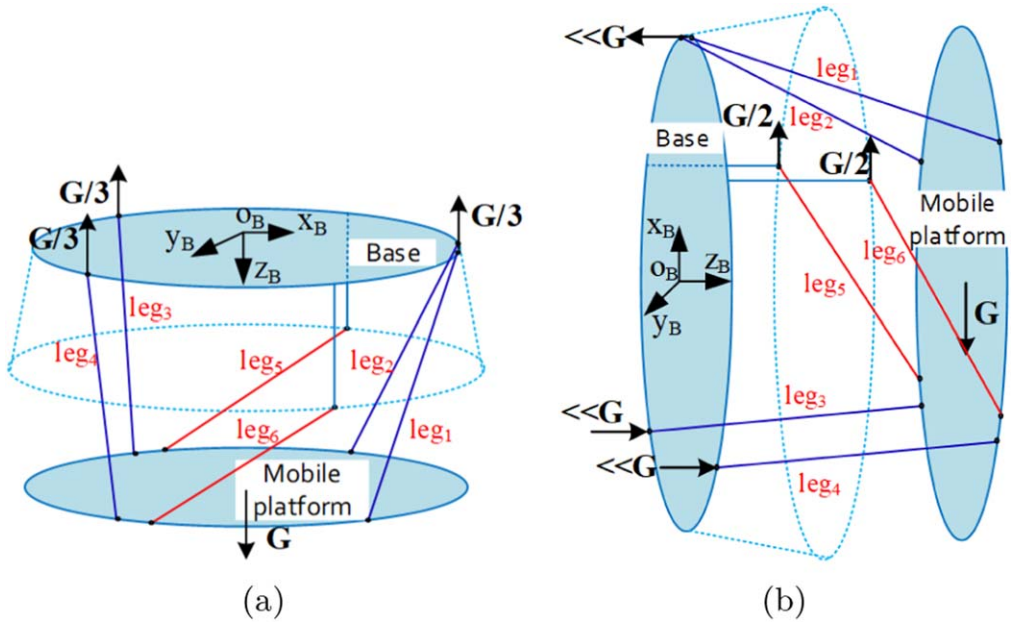

Figure 4. The modified Stewart platform. (a) Forces on actuator mount point in zenith position; (b) Forces on actuator mount point in horizon position.

Here $\boldsymbol{G}_f^F$ is the transpose of the Jacobian matrix $\boldsymbol{J}$. When $\boldsymbol{G}_f^F$ is not singular

$$\boldsymbol{f} = \boldsymbol{G}_F^f \cdot \boldsymbol{F}, \tag{7}$$

where $\boldsymbol{G}_F^f = (\boldsymbol{G}_f^F)^{-1}$. Considering that the modified Stewart platform will move along with the antenna system, and gravity loads vary within the static configuration at different elevation angles, the elevation axis of the antenna y_w is parallel to the y_B axis of the base frame, that is

$$\boldsymbol{f} = \boldsymbol{G}_F^{\mathrm{f}} \cdot \boldsymbol{R}_\varphi \cdot \boldsymbol{F}, \tag{8}$$

where $\boldsymbol{R}_\varphi = \begin{bmatrix} \boldsymbol{T}_\varphi & \\ & \boldsymbol{T}_\varphi \end{bmatrix}$, $\boldsymbol{T}_\varphi = \begin{bmatrix} \cos\varphi & 0 & \sin\varphi \\ 0 & 1 & 0 \\ -\sin\varphi & 0 & \cos\varphi \end{bmatrix}$ and φ is the elevation angle of the radio telescope.

4.2. Stiffness Performance Evaluation Indices of the Modified Stewart Platform

Suppose that the rigid mobile platform is elastically suspended by six elastic active legs. If only small displacements from its unpreloaded equilibrium position are considered, the overall force-deformation relation of the mechanism is linearly elastic. When each of the reacting forces $\boldsymbol{f} = [f_1\, f_2\, f_3\, f_4\, f_5\, f_6]^T$ is applied to leg i and along the axial direction, the longitudinal elastic differential deformation $\boldsymbol{\delta} = [\delta_1\, \delta_2\, \delta_3\, \delta_4\, \delta_5\, \delta_6]$ can be solved as follows

$$\boldsymbol{\delta} = \frac{\boldsymbol{f}}{\boldsymbol{K}_{\mathrm{p}}}, \tag{9}$$

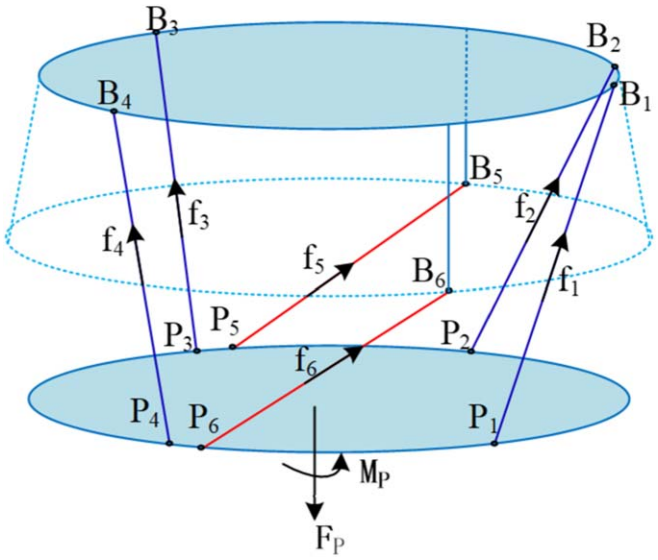

Figure 5. Schematic diagram of the load.

where K_p is a 6×6 symmetric axial stiffness matrix of the legs

$$\boldsymbol{K}_{\mathrm{p}} = \begin{bmatrix} \mathrm{k}_{p1} & & & & & 0 \\ & \mathrm{k}_{p2} & & & & \\ & & \mathrm{k}_{p3} & & & \\ & & & \mathrm{k}_{p4} & & \\ & & & & \mathrm{k}_{p5} & \\ 0 & & & & & \mathrm{k}_{p6} \end{bmatrix}_{6\times 6}. \tag{10}$$

Here k_{pi} is the axial stiffness of leg i

$$k_{pi} = \frac{\pi E d_i^2}{4L_i}, \tag{11}$$

and E is the modulus of elasticity for the leg, L_i is the length of leg i, and d_i is the equivalent cross-section diameter of leg i. The legs of the modified Stewart platform are symmetrically distributed in pairs, $d_1 = d_2$, $d_3 = d_4$, $d_5 = d_6$, so the axial stiffness of the leg $k_{p1} = k_{p2}$, $k_{p3} = k_{p4}$, $k_{p5} = k_{p6}$.

Based on the theorem of work and energy being equal to each other, the sum of the deformation energy produced by forces $\boldsymbol{f}$ and the deformation work produced by force $\boldsymbol{F}$ applied on the mobile platform must be zero. This implies that the elastic differential deformation of the mobile platform can be represented by three translational components, dx, dy, and dz, as well as three rotational components, $d\alpha$, $d\beta$ and $d\gamma$. Thus, there is

$$\begin{bmatrix} \delta_1 \\ \delta_2 \\ \delta_3 \\ \delta_4 \\ \delta_5 \\ \delta_6 \end{bmatrix}^T \begin{bmatrix} \boldsymbol{f}_1 \\ \boldsymbol{f}_2 \\ \boldsymbol{f}_3 \\ \boldsymbol{f}_4 \\ \boldsymbol{f}_5 \\ \boldsymbol{f}_6 \end{bmatrix} = - \begin{bmatrix} dx \\ dy \\ dz \\ d\alpha \\ d\beta \\ d\gamma \end{bmatrix}^T \boldsymbol{F}, \tag{12}$$

and from inverse kinematics, it can be obtained that

$$\begin{bmatrix} \delta_1 \\ \delta_2 \\ \delta_3 \\ \delta_4 \\ \delta_5 \\ \delta_6 \end{bmatrix} = \boldsymbol{J} \begin{bmatrix} dx \\ dy \\ dz \\ d\alpha \\ d\beta \\ d\gamma \end{bmatrix}. \tag{13}$$

From Equations (9), (12) and (13) we can get

$$\boldsymbol{F} = -\boldsymbol{J}^T \boldsymbol{K}_P \boldsymbol{J} \begin{bmatrix} dx \\ dy \\ dz \\ d\alpha \\ d\beta \\ d\gamma \end{bmatrix}. \tag{14}$$

Let $\boldsymbol{K} = (-\boldsymbol{J}^T \boldsymbol{K}_P \boldsymbol{J})_{6\times 6}$, and $\boldsymbol{K}$ be a 6×6 symmetric stiffness matrix. When supporting workload $\boldsymbol{F}$, the forward elastic deformation of the modified Stewart platform can be solved as

$$\begin{bmatrix} dx \\ dy \\ dz \\ d\alpha \\ d\beta \\ d\gamma \end{bmatrix} = \boldsymbol{K}^{-1} \boldsymbol{F}. \tag{15}$$

Let $\boldsymbol{X} = [dx, dy, dz, d\alpha, d\beta, d\gamma]$, then the stiffness performance evaluation indices are

$$\boldsymbol{P}(\boldsymbol{X}) = \frac{||\boldsymbol{F}||_2}{||\boldsymbol{X}||_2} = \frac{\boldsymbol{F}^T \boldsymbol{F}}{(\boldsymbol{K}^{-1}\boldsymbol{F})^T (\boldsymbol{K}^{-1}\boldsymbol{F})^T}. \tag{16}$$

5. Comprehensive Index Optimization of the Modified Stewart Platform

To optimize the modified Stewart platform during conceptual design, dimensional and structural parameters are obtained by simplifying the parts to a permissible level. Linkages are treated as standard beam elements and the mobile platform is assumed to have a regular shape, which is acceptable at this stage. Refinement of each part can be carried out after the optimization process.

5.1. Optimized Dimensional Parameters

In order to determine the optimal dimensional parameters for the modified Stewart platform, it is crucial to carefully select appropriate design variables. The design parameters, denoted as $\boldsymbol{x} = [r_{B1}, r_{B2}, h_B, h_{PB}, \alpha_1 \sim \alpha_6]$, consist of several key variables. As shown in Figure 6, r_{B1} and r_{B2} represent the radii of the base platform, h_B is the distance between the base platform and attachment point B_5B_6, h_{PB} is the distance between the base platform and the mobile platform, and $\alpha_1 \sim \alpha_6$ are the angles between the x-axis and attachment points B_i and P_i. Additionally, r_P represents the radius of the mobile platform and is determined by the antenna structure. Once these variables are determined, the positions of the attachment points can be easily computed in the Cartesian space as a function of the design parameters as expressed below:

$$\begin{aligned}
\boldsymbol{B}_1^B &= [r_{B1}\cos(\alpha_1), r_{B1}\sin(\alpha_1), 0]^T \\
\boldsymbol{B}_2^B &= [r_{B1}\cos(-\alpha_1), r_{B1}\sin(-\alpha_1), 0]^T \\
\boldsymbol{B}_3^B &= [-r_{B1}\cos(-\alpha_2), r_{B1}\sin(-\alpha_2), 0]^T \\
\boldsymbol{B}_4^B &= [-r_{B1}\cos(\alpha_2), r_{B1}\sin(\alpha_2), 0]^T \\
\boldsymbol{B}_5^B &= [r_{B2}\cos(-\alpha_3), r_{B2}\sin(-\alpha_3), h_B]^T \\
\boldsymbol{B}_6^B &= [r_{B2}\cos(\alpha_3), r_{B2}\sin(\alpha_3), h_B]^T \\
\boldsymbol{P}_1^P &= [r_P\cos(\alpha_4), r_P\sin(\alpha_4), 0]^T \\
\boldsymbol{P}_2^P &= [r_P\cos(-\alpha_4), r_P\sin(-\alpha_4), 0]^T \\
\boldsymbol{P}_3^P &= [-r_P\cos(-\alpha_5), r_P\sin(-\alpha_5), 0]^T \\
\boldsymbol{P}_4^P &= [-r_P\cos(\alpha_5), r_P\sin(\alpha_5), 0]^T \\
\boldsymbol{P}_5^P &= [-r_P\cos(-\alpha_6), r_P\sin(-\alpha_6), 0]^T \\
\boldsymbol{P}_6^P &= [-r_P\cos(\alpha_6), r_P\sin(\alpha_6), 0]^T
\end{aligned}.$$

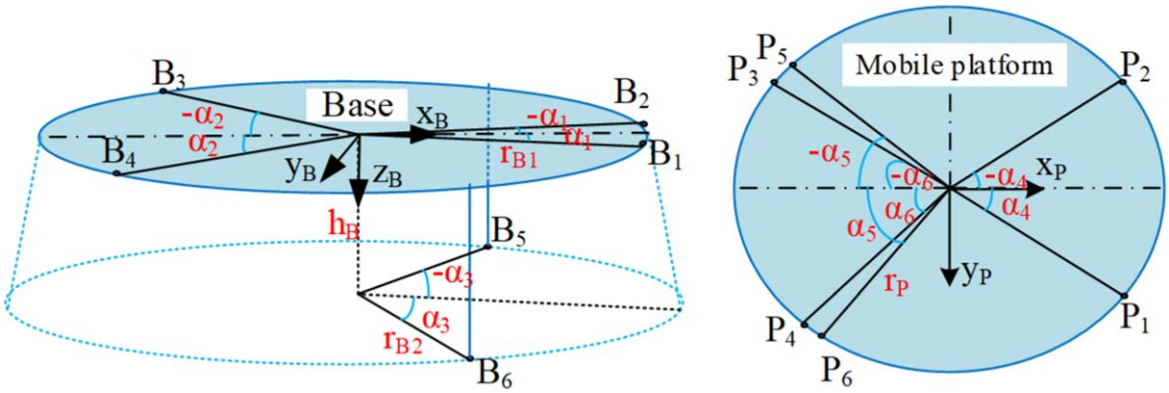

Figure 6. Modified Stewart platform geometric design parameters.

5.1.1. The Cost Function

In order to effectively adjust the position of the sub-reflector, the modified Stewart platform must be capable of following the primary reflector as it elevates from 5° to 88°. Additionally, due to the heavy load (⩾4000 kg) that the platform must support, it is crucial to carefully consider the forces that will be placed on the legs of the Stewart platform.

To address this concern, the primary objective is to minimize the maximum leg force value in the workspace while the primary reflector (base platform) elevates from 5° to 88°

$$w_1(\boldsymbol{x}) = \min(\max(\boldsymbol{G}_{\boldsymbol{F}}^{\mathrm{f}} \cdot \boldsymbol{R}_{\varphi} \cdot \boldsymbol{F})), \tag{17}$$

where $\boldsymbol{F} = [m\boldsymbol{g}, \boldsymbol{q}^{B} \times m\boldsymbol{g}]$, $\boldsymbol{g} = [0, 0, 9.8]\ \mathrm{m\,s^{-2}}$, $m = 4000\ \mathrm{kg}$ and $5 \leqslant \varphi \leqslant 88$. This will help to ensure the stability and reliability of the platform, even under heavy load and during significant changes in position.

The manipulability index value based on the traditional Jacobian matrix indirectly represents the maximum positioning error of the modified Stewart platform. A smaller manipulability index value indicates a larger maximum positioning error. Therefore, the secondary objective is to minimize the condition number of the kinematic Jacobian matrix under all working conditions to achieve greater accuracy and reliability

$$w_1(\boldsymbol{x}) = \min(\mathrm{cond}\boldsymbol{J}). \tag{18}$$

The cost function can be expressed as the following:

Minimize $[\max(\boldsymbol{G}_{\boldsymbol{F}}^{\mathrm{f}} \cdot \boldsymbol{R}_{\varphi} \cdot \boldsymbol{F}), \mathrm{cond}\boldsymbol{J}]$

Subject to $l_{\mathrm{i,min}} \leqslant l_i \leqslant l_{\mathrm{i,max}}$; $\alpha_{\mathrm{i,min}} \leqslant \alpha_i \leqslant \alpha_{\mathrm{i,max}}$; $r_{B1} \leqslant r_{B2}$; $r_{B2} \leqslant r_P$; $h_B \leqslant h_{\mathrm{PB}}$; $\alpha_4 \leqslant \alpha_3$; $\alpha_6 \leqslant \alpha_5$; $r_P = 1555$ mm.

Moreover, $l_{\mathrm{i,min}} = \frac{2}{3} l_{i0}$, $l_{\mathrm{i,max}} = \frac{4}{3} l_{i0}$ and l_{i0} is the length of leg i while the mobile platform is at the zero position. The upper and lower limits of the design parameters are listed in Table 2.

Table 2
Upper and Lower Limits of the Design Parameters

	r_{B1}	r_{B2}	h_B	r_{PB}	$\alpha_1 \sim \alpha_6$
Lower limits (mm)	r_P	r_P	0	1000	5°
Upper limits (mm)	3000	3000	3000	3000	90°

5.1.2. Optimized Result

By carefully optimizing the design and considering the various design variables, it is possible to achieve a modified Stewart platform that is both robust and highly effective for its intended purpose. The optimization of the dimensional parameters of the modified Stewart platform is a nonlinear programming problem. To address this, NSGA-II is utilized as an effective optimization algorithm. The results of the optimization are presented in Table 3.

5.2. Optimized Section Parameters of the Links

The ability of the Stewart platform to resist deformation under external load is crucial for its accuracy, particularly when it comes to bearing heavy loads. This property, also known as stiffness performance, is essential for the proper functioning of the Stewart platform for QTT.

The modified Stewart platform is supported by four orthogonal supporting legs installed at QTT, and when subjected to larger loads, the supporting legs tend to deform, resulting in a sub-reflector offset. To enhance the platform's stiffness and reduce its mass, this part optimizes the section parameters of the links, with a primary focus on stiffness and mass properties, based on the optimized dimensional parameters mentioned above.

Throughout the design process, the linkage of the modified Stewart platform can be regarded as a standard spatial beam element or an assembly of such elements. The platform's actuators are symmetrically distributed about the x_B-axis, and

Table 3
Upper and Lower Limits of the Design Parameters

r_{B1}/mm	r_{B2}/mm	h_B/mm	r_{PB}/mm	α_1	α_2	α_3	α_4	α_5	α_6
2709.15	2885.22	1280.37	2038.96	5°	37°.4	59°.1	39°.0	58°.6	63°.6

their parameters are equal in pairs. Therefore, the platform's design variables are represented as $\boldsymbol{d} = [d_1,\ d_2,\ d_3]$, with $d_m (m = 1,\ 2,\ 3)$ representing the equivalent cross-sectional diameter of the six legs. Both the static stiffness index and mass matrix of the platform are affected by the aforementioned design variables.

5.2.1. The Cost Function

The corresponding objective functions can be defined based on the static stiffness indices mentioned above

$$w_3(\boldsymbol{d}) = \min\left(\frac{\int\int \boldsymbol{P}(\boldsymbol{X}) ds d\varphi}{\int\int ds d\varphi}\right), \tag{19}$$

where s is the required workspace of the QTT as shown in Table 1, φ is the elevation angle of the radio telescope and $5 \leqslant \varphi \leqslant 88$.

The mass in motion of the modified Stewart platform is determined by the dimensions of its mechanism. The mass of each component can be easily calculated based on its geometry and the density of the material used. Therefore, the objective function for mass performance can be expressed as follows

$$w_4(\boldsymbol{d}) = \min(2\rho(\upsilon_1(d_1) + \upsilon_2(d_2) + \upsilon_3(d_3))), \tag{20}$$

where ρ is mass density of the material used to construct the modified Stewart platform, and $\upsilon_m(d_m)$ is the volume function of the leg.

The cost function can be expressed as:

Minimize $\left[\frac{\int\int \boldsymbol{P}(\boldsymbol{X}) ds d\varphi}{\int\int ds d\varphi},\ 2\rho(\upsilon_1(d_1) + \upsilon_2(d_2) + \upsilon_3(d_3))\right]$

Subject to $d_{\mathrm{m,min}} \leqslant d_i \leqslant d_{\mathrm{m,max}}$; $\sigma_m \leqslant [\sigma]$.

The stress of each leg of the modified Stewart platform must be less than the allowable stress of its material $[\sigma]$.

5.2.2. Optimization Result

NSGA-II is employed as the optimization algorithm for the nonlinear programming function. The optimization results in a solution represented by $\boldsymbol{d} = [75.72\ \mathrm{mm},\ 111.42\ \mathrm{mm},\ 88.31\ \mathrm{mm}]$. To visually represent the optimized design, a three-dimensional solid model of the modified Stewart platform is generated based on the obtained results, as drawn in Figure 7.

6. Performance Comparisons

During the mechanical design phase of the sub-reflector actuator for the QTT, the primary evaluation indices include

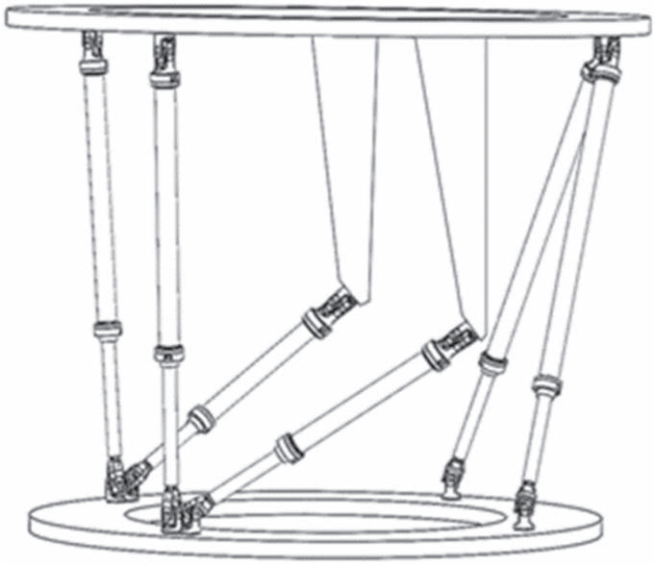

Figure 7. Three-dimensional solid model of the modified Stewart platform.

static load capacity and stiffness. In this section, a comparison is made between the performance of the traditional Stewart platform, designed for the 65 m Tianma Radio Telescope (Yao et al. 2016), and the modified Stewart platform with regard to the aforementioned evaluation indices. This comparison provides insights into the effectiveness of the modifications made to the design of the Stewart platform for the QTT.

Figure 8 depicts the actuator loads while the radio telescope's elevation angle ranges from 5° to 88° at the zero position. The reaction forces on the traditional Stewart platform's leg range from −20.1 to 16.1 kN. As the elevation angle decreases larger actuator loads are needed to maintain the same level of load, and over the entire elevation angle range of 5°–88°, the force direction of the four legs changes. On the other hand, the reaction forces on the modified Stewart platform's leg range from −18.9 to 15.8 kN, the force changes uniformly across the entire elevation angles and only two legs change their force direction. This suggests that four legs always maintain unidirectional force, which eliminates the possibility of producing an error due to a change in the direction of force. Consequently, the modified Stewart platform exhibits better static load-bearing capacity.

To determine the stiffness performance of both traditional and modified Stewart platforms, static stiffness was measured at elevation angles of $\varphi = 90$ and $\varphi = 0$ over the working plane

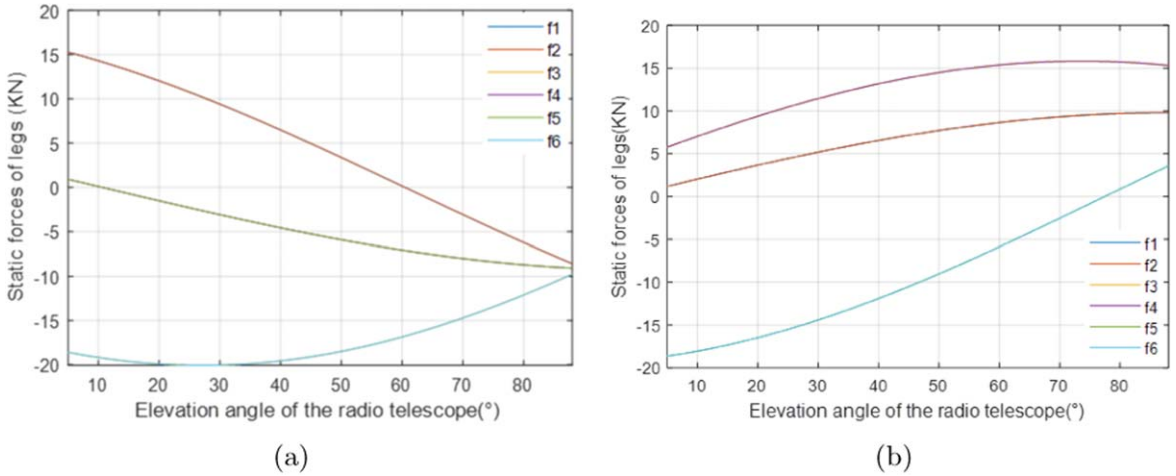

Figure 8. Variations of actuator loads of (a) the traditional Stewart platform where $f_1 = f_2, f_3 = f_6, f_4 = f_5$ and (b) the modified Stewart platform where $f_1 = f_2, f_3 = f_4$, $f_5 = f_6$ with respect to the elevation angle of the radio telescope.

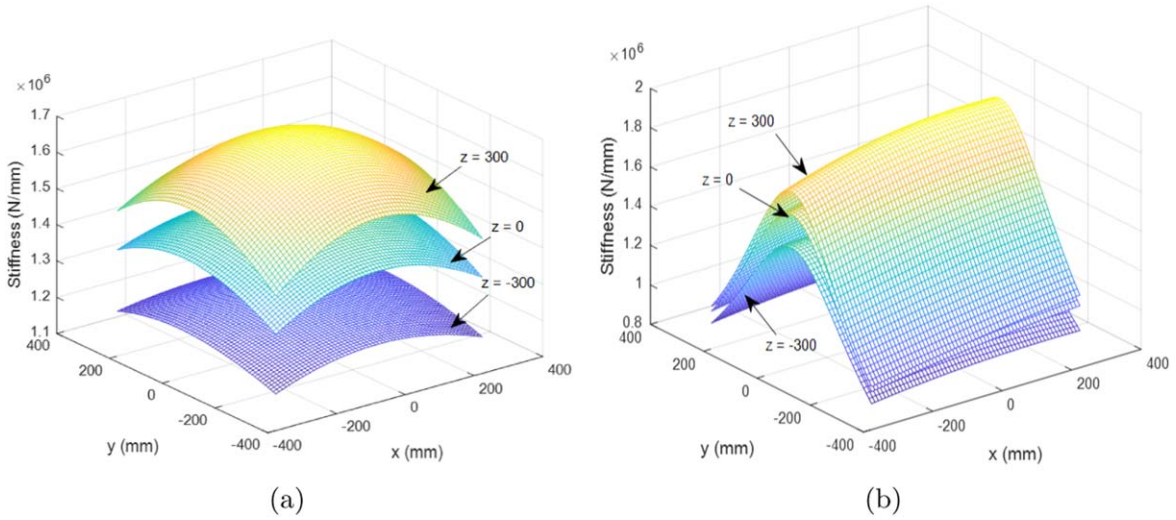

Figure 9. Distributions of global stiffness of (a) the traditional Stewart platform and (b) the modified Stewart platform over the working plane $z = -300$ mm, 0 mm and 300 mm while the elevation angle is 90°.

$z = -300$ mm, 0 mm, and 300 mm. As affirmed in Figures 9 and 10, the stiffness range of the traditional Stewart platform falls between 1.15×10^3 and 1.68×10^3 kN mm^{-1} at $\varphi = 90$, and 4.50×10^2–7.02×10^2 kN mm^{-1} at $\varphi = 0$. On the other hand, the modified Stewart platform exhibits a stiffness range of 9.10×10^2–1.86×10^3 kN mm^{-1} at $\varphi = 90$, and $9.41 \times 10^2 \sim 1.16 \times 10^3$ kN mm^{-1} at $\varphi = 0$.

The traditional Stewart platform shows poor stiffness performance at $\varphi = 0$, as its minimum stiffness is almost half that of the modified Stewart platform. Moreover, the stiffness variation range of the traditional Stewart platform over the full elevation range and working space is 1.23×10^3 kN mm^{-1}, while that of the modified Stewart platform is only 9.5×10^2 kN mm^{-1}. In other words, the modified Stewart platform demonstrates a more uniform stiffness distribution across the full elevation range, indicating superior stiffness performance overall.

7. Conclusions

In conclusion, this paper proposes a modified Stewart platform with two separated actuators as an efficient sub-reflector actuator for radio telescopes. The proposed design offers accurate adjustment of the sub-reflector position while moving in elevation together with the primary reflector. Through performance analysis and optimization, it has been demonstrated that the modified platform outperforms the traditional Stewart platform in terms of static load-bearing capacity and stiffness.

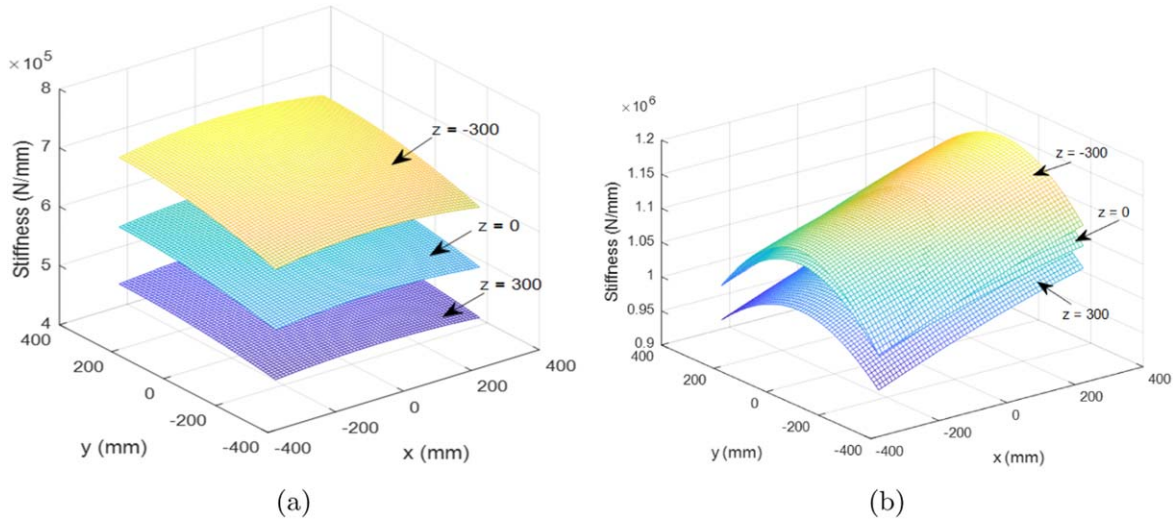

Figure 10. Distributions of global stiffness of (a) the traditional Stewart platform and (b) the modified Stewart platform over the working plane $z = -300$ mm, 0 mm and 300 mm while the elevation angle is 0°.

Specifically, the actuator loads of the modified platform are consistently lower and more uniformly distributed than those of the traditional platform across the entire elevation angle, and display a more uniform stiffness distribution. In contrast, the traditional Stewart platform exhibits weak stiffness and load-bearing capacity at low elevation angles. Based on these findings, the modified Stewart platform is a choice for sub-reflector actuators in radio telescopes and provides improved stability and precision during operation. Future research could explore practical implementation and further advancements of this design to enhance radio telescope technology.

Acknowledgments

This study was supported by the National Natural Science Foundation of China (NSFC, grant No. 12203095), the Youth Innovation Promotion Association, CAS (No. Y202019), Natural Science Foundation of Xinjiang Uygur Autonomous Region (No. 2022D01B220), Tianchi Doctoral Program 2021 and the Scientific Instrument Developing Project of the Chinese Academy of Sciences (No. PTYQ2022YZZD01).

References

Chen, H., Feng, Z., Liu, Y., et al. 2023, J. Const. Eng. Manag., 149, 04022169
Cirillo, A., Cirillo, P., De Maria, G., et al. 2017, Rob. Comput. Integr. Manuf., 44, 1
Gawronski, W., & Souccar, K. 2005, IAPM, 47, 41
Hamida, I. B., Laribi, M. A., Mlika, A., et al. 2021, Mech. Mach. Theory, 156, 104141
Jiang, M., Rui, X., Zhu, W., Yang, F., & Zhang, Y. 2021, AcMSn, 37, 127
Keshtkar, S., Hernandez, E., Oropeza, A., & Poznyak, A. 2017, Neurocom., 233, 43
Li, J. J., Duan, Y. B., Zeng, D. X., & Zhao, Y. S. 2014, J. Syst. Simulation, 26, 8, (in Chinese)
Liu, G., Qu, Z., Han, J., & Liu, X. 2013, Industrial Robot: An Int. J., 40, 550
Merlet, J.-P. 2006, Parallel Robots (Berlin: Springer)
Nayar, H., Goel, A., Boettcher, A., et al. 2021, Earth and Space, 2021, 531
Nunez, D. A., Mauledoux, M., Aviles, O., Guacheta, J., & Gonzalez, S. 2022, Int. J. Mech. Eng. Robot. Res., 11, 4
Pietzner, J., & Nothnagel, A. 2010, in EGU General Assembly Conf. Abstracts, 12 (Vienna: EGU General Assembly), 11214
Prestage, R. M., & Maddalena, R. J. 2006, in Conf. on Ground-based and Airborne Telescopes (Bellingham, WA: SPIE)
Stoughton, R. S., & Arai, T. 1993, IEEE Trans. Robot. Autom., 9, 166
Su, Y. X., & Duan, B. Y. 2000, J. Robot. Syst., 17, 375
Sun, T., & Lian, B. 2018, MeMaT, 120, 73
Toz, M., & Kucuk, S. 2013, Rob. Autom. Syst., 61, 1516
Wang, C. S., Yan, Y. F., Xu, Q., et al. 2020, RAA, 20, 10
Wang, N. 2014, SSPMA, 44, 783
Wootten, A., & Thompson, A. R. 2009, Proc. IEEE, 97, 1463
Xiang, B. B., Wang, C. S., Lian, P. Y., Wang, N., & Ban, Y. 2019, RAA, 19, 062
Xu, Q., & Wang, N. 2016, Proc. SPIE, 9906, 99065L
Xu, Q., Li, L., & Cheng, A. Y. 2015, Trans. Tech. Publ., 741, 61
Yao, J.-T., Zeng, D., Hou, Y., et al. 2016, Manned Spaceflight, 22, 69, (in Chinese)